The Journal of Neuroscience, October 15, 1998, 18(20):8111–8125

Functional and Molecular Differences between Voltage-Gated K$^+$ Channels of Fast-Spiking Interneurons and Pyramidal Neurons of Rat Hippocampus

Marco Martina,[1] Jobst H. Schultz,[2] Heimo Ehmke,[2] Hannah Monyer,[3] and Peter Jonas[1]

[1]Physiologisches Institut der Universität Freiburg, D-79104 Freiburg, Germany, [2]Physiologisches Institut der Universität Heidelberg, D-69120 Heidelberg, Germany, and [3]Zentrum für Molekulare Biologie der Universität Heidelberg, D-69120 Heidelberg, Germany

We have examined gating and pharmacological characteristics of somatic K$^+$ channels in fast-spiking interneurons and regularly spiking principal neurons of hippocampal slices. In nucleated patches isolated from basket cells of the dentate gyrus, a fast delayed rectifier K$^+$ current component that was highly sensitive to tetraethylammonium (TEA) and 4-aminopyridine (4-AP) (half-maximal inhibitory concentrations <0.1 mM) predominated, contributing an average of 58% to the total K$^+$ current in these cells. By contrast, in pyramidal neurons of the CA1 region a rapidly inactivating A-type K$^+$ current component that was TEA-resistant prevailed, contributing 61% to the total K$^+$ current. Both types of neurons also showed small amounts of the K$^+$ current component mainly found in the other type of neuron and, in addition, a slow delayed rectifier K$^+$ current component with intermediate properties (slow inactivation, intermediate sensitivity to TEA). Single-cell RT-PCR analysis of mRNA revealed that Kv3 (Kv3.1, Kv3.2) subunit transcripts were expressed in almost all (89%) of the interneurons but only in 17% of the pyramidal neurons. In contrast, Kv4 (Kv4.2, Kv4.3) subunit mRNAs were present in 87% of pyramidal neurons but only in 55% of interneurons. Selective block of fast delayed rectifier K$^+$ channels, presumably assembled from Kv3 subunits, by 4-AP reduced substantially the action potential frequency in interneurons. These results indicate that the differential expression of Kv3 and Kv4 subunits shapes the action potential phenotypes of principal neurons and interneurons in the cortex.

Key words: interneurons; voltage-gated K$^+$ channels; Kv1, Kv2, Kv3, Kv4 subunits; nucleated patch; single-cell RT-PCR; hippocampal slices

Cortical neurons differ in the intrinsic pattern of action potentials they generate on sustained current injection (for review, see Connors and Gutnick, 1990). Glutamatergic principal neurons in the hippocampus are regularly spiking or intrinsically bursting and show adaptation (Madison and Nicoll, 1984), whereas several types of GABAergic interneurons are fast-spiking and generate high-frequency trains of action potentials (Han et al., 1993; Scharfman, 1995). The specific functional properties of ion channels that confer the different action potential phenotypes are not entirely understood. K$^+$ channels of both delayed rectifier-type and inactivating A-type were found in fast-spiking interneurons in stratum oriens-alveus of the hippocampal CA1 region (Zhang and McBain, 1995a,b); the main difference to the K$^+$ current in principal neurons (Numann et al., 1987; Ficker and Heinemann, 1992; Storm, 1990) appeared to be the faster activation time course of the delayed rectifier component. Delayed rectifier K$^+$ channels with rapid activation and deactivation were also identified in interneurons of CA1 stratum pyramidale. Low concentrations of 4-AP and TEA blocked the delayed rectifier component in interneurons of stratum pyramidale (Du et al., 1996) but not in those of stratum oriens-alveus (Zhang and McBain, 1995a). The functional impact of these pharmacologically distinct K$^+$ channels on the discharge patterns of various interneurons remains to be addressed.

The K$^+$ channel subunit expression profile of fast-spiking interneurons is also unclear. Native voltage-gated K$^+$ channels are multimeric proteins assembled from pore-forming α subunits and auxiliary β subunits. The α subunits of rat K$^+$ channels are encoded by four main subfamilies of genes (Kv1, Kv2, Kv3, and Kv4), which are homologous to the Shaker, Shab, Shaw, and Shal genes in *Drosophila* (Chandy, 1991). Previous studies showed that Kv3.1 subunits are expressed preferentially in parvalbumin-positive interneurons in the hippocampus (Weiser et al., 1995; Du et al., 1996), but several observations raise doubts that Kv3.1 is the only determinant of the fast-spiking phenotype. First, regularly spiking pyramidal neurons in the hippocampus also express Kv3.1 mRNA (Weiser et al., 1994). Second, somatostatin-positive interneurons in the stratum oriens-alveus do not express Kv3.1 protein (Du et al., 1996). Third, *in situ* hybridization and immunocytochemical analysis indicated that scattered cells throughout the hippocampus, perhaps corresponding to specific interneuron subtypes, were also positive for Kv3.2/3.3 (Weiser et al., 1994), Kv2 (Maletic-Savatic et al., 1995), and Kv4 subunits (Tsaur et al., 1997; Serôdio and Rudy, 1998). Finally, Kv3.1-deficient mice do not develop spontaneous seizures, contrary to what is expected if Kv3.1 were the key determinant of the fast-spiking phenotype (Ho et al., 1997). Thus, a complete molecular characterization of the K$^+$ channel repertoire of defined interneuron subtypes is

Received April 24, 1998; revised July 23, 1998; accepted July 30, 1998.

Supported by German Israeli Foundation Grant I 0352–073.01/94 to P.J. and Deutsche Forschungsgemeinschaft Grant Mo 432/3–1 to H.M. We thank Drs. L. Y. Jan, D. McKinnon, O. Pongs, L. Salkoff, S. H. Snyder, and J. S. Trimmer for providing plasmids, Dr. D. J. Surmeier for sharing unpublished data, and Drs. J. Bischofberger and J. R. P. Geiger for critically reading this manuscript.

M.M. and J.H.S. contributed equally to this work.

Correspondence should be addressed to Dr. Peter Jonas, Physiologisches Institut, Universität Freiburg, Hermann-Herder-Strasse 7, D-79104 Freiburg, Germany.

 0270-6474/98/188111-15$05.00/0

required before final conclusions regarding the molecular basis of their intrinsic discharge patterns can be reached.

To address this issue, we compared the functional and molecular properties of K^+ channels in a prototypic fast-spiking GABAergic interneuron (the dentate gyrus basket cell, BC) and a regularly spiking glutamatergic principal neuron (the CA1 pyramidal cell, PC). The results suggest that differential expression of Kv3 and Kv4 subunit genes is a main factor shaping the intrinsic discharge patterns of hippocampal neurons.

MATERIALS AND METHODS

Cell identification and recording of K^+ currents from nucleated patches. Transverse hippocampal slices of 300 μm thickness were cut from the brains of 11- to 16-d-old Wistar rats using a Vibratome (Dosaka, Kyoto, Japan). Animals were killed by decapitation, in agreement with national and institutional guidelines. Basket cells in the dentate gyrus and pyramidal neurons in the hippocampal CA1 subfield were identified visually using infrared differential interference contrast (IR-DIC) videomicroscopy. Basket cells were identified on the basis of the following criteria: large size and pyramidal or fusiform shape of the soma, location of the soma at the border between granule cell layer and hilus, and orientation of the apical dendrite perpendicular to the granule cell layer. Putative interneurons were only accepted when the action potential frequency on sustained injection of depolarizing current (0.5 or 1 sec, 100–400 pA) exceeded 60 Hz at ~22°C (Han et al., 1993). Patch pipettes were pulled from borosilicate glass tubing (2.0 mm outer diameter, 0.5 mm wall thickness) and heat-polished before use. The pipette resistance ranged from 2 to 5 MΩ, and the series resistance in the whole-cell configuration was 4–14 MΩ. Only neurons with initial resting potentials negative to −55 mV were accepted. To isolate nucleated patches, negative pressure (50–150 mbar) was applied, and the patch pipette was withdrawn slowly; a small negative pressure (10–20 mbar) was kept during recording. Nucleated patches had input resistances of 2–5 GΩ; their shape was spherical, and the diameter was 8.6 ± 0.5 μm, independent of the cell type. Previous estimates indicate that the nucleated patch membrane follows a command voltage step with a time constant <50 μsec (Martina and Jonas, 1997).

All measurements were made from nucleated patches, except the current-clamp recordings of action potential patterns that were obtained in the whole-cell configuration (see Figs. 1*A*,*B*, 9*A*,*B*). An Axopatch 200A amplifier (Axon Instruments, Foster City, CA) that included a bridge-balance circuit for series resistance compensation in current-clamp mode was used for measurements. Signals were filtered at 5 or 10 kHz using the 4-pole low-pass Bessel filter, and capacitive transients were reduced by the compensation circuit of the amplifier. A 1401plus interface (Cambridge Electronic Design, Cambridge, England) connected to a personal computer was used for stimulus generation and data acquisition. The sampling frequency was 10 or 20 kHz.

Nucleated patches were held at −90 mV. Pulse sequences were generated by homemade programs that also allowed us to apply previously recorded waveforms as voltage-clamp commands. Leakage and capacitive currents were subtracted on-line using a "P over −4" procedure (Martina and Jonas, 1997). Current components sensitive to a blocker were determined off-line by direct subtraction of raw traces. Na^+ currents, when apparent, were blocked by adding 0.3 or 0.5 μM tetrodotoxin (TTX; Sigma, St. Louis, MO) to the external solution. Traces shown in the figures represent single sweeps or averages from up to 10 sweeps. Test pulses were applied every 4–5 sec, except when the recovery from inactivation was studied (see Fig. 6*G*,*H*; time interval between pulse sequences, 20 sec). Test pulses were continuously applied during and after wash-in of TEA, 4-AP, or dendrotoxin (DTX), and final recordings were made in steady-state conditions. The washout of the blockers was also examined; the effects were almost completely (TEA, <1 mM 4-AP) or partially (≥1 mM 4-AP) reversible. No correction for liquid junction potentials was made. The electrophysiological data included in this study were obtained from 80 BC patches and 66 PC patches. All recordings were made at room temperature (20–24°C).

Solutions and chemicals. Slices were superfused with physiological extracellular solution containing (in mM): 125 NaCl, 25 $NaHCO_3$, 2.5 KCl, 1.25 NaH_2PO_4, 2 $CaCl_2$, 1 $MgCl_2$, and 25 glucose, bubbled with 95% O_2 and 5% CO_2. 4-AP (Sigma) and TEA (Merck, Darmstadt, Germany) were applied to nucleated patches either via bath superfusion or using a multi-barrelled application pipette. α-Dendrotoxin (Alomone, Jerusalem, Israel) was applied exclusively with the application pipette. Application pipette barrels were continuously perfused with a Na^+-rich solution containing (in mM): 135 NaCl, 5.4 KCl, 1.8 $CaCl_2$, 1 $MgCl_2$, and 5 HEPES, pH-adjusted to 7.2 with NaOH; in the experiments with DTX, 0.1% bovine serum albumin was added. Recording pipettes were filled with K^+-rich internal solution, containing (in mM): 140 KCl, 10 EGTA, 2 $MgCl_2$, 2 Na_2ATP, 2 glutathione-SH, and 10 HEPES, pH-adjusted to 7.3 with KOH. In some experiments, glutathione-SH was omitted. All chemicals were from Merck or Sigma, unless specified differently.

Analysis. Traces and data points were fitted using a nonlinear least-squares algorithm. To obtain the activation curve, values of chord conductance (G) were calculated from the respective peak currents, assuming ohmic behavior and a reversal potential of −95 mV. This potential was close to the experimentally determined reversal potentials of tail currents, which were −98.8 ± 2.0 mV in BC patches ($n = 6$) and −96.4 ± 5.0 mV in PC patches ($n = 3$). Activation and inactivation curves were fitted with functions based on the Boltzmann equation $f = 1/\{1 + \exp[\pm(V\text{-}V_{1/2})/k]\}$, where V is the membrane potential, $V_{1/2}$ is the potential at which the value of the Boltzmann function is 0.5, and k is the slope factor. The activation curves were fitted with a Boltzmann function raised to the fourth power; the midpoint potentials given indicate the potential at which the conductance reached the half-maximal value. Data are reported as mean ± SEM; error bars in Figures also represent SEM and were plotted only when they exceeded the respective symbol size. Statistical significance was assessed using a two-sided t test for paired or unpaired samples at the significance level (P) indicated. Figures show data pooled from different patches. SEs of fitted parameters were obtained by analyzing data of individual experiments separately.

Single-cell RT-PCR. Methods for single-cell RT-PCR were similar to those described previously (Monyer and Jonas, 1995). Patch pipettes used for RT-PCR experiments (0.8–3 MΩ) were filled with autoclaved internal solution containing (in mM): 140 KCl, 5 EGTA, 3 $MgCl_2$, and 5 HEPES, pH-adjusted to 7.3 with KOH. The cytoplasm of a whole-cell recorded neuron, either including (Kv2, Kv3, and Kv4) or excluding (Kv1) the nucleus, was harvested into the patch pipette by applying negative pressure. The harvested material was then expelled under visual control into an autoclaved reaction tube containing hexamer random primers, deoxyribonucleoside triphosphates, dithiothreitol, ribonuclease inhibitor, and Superscript reverse transcriptase II (Life Technologies, Gaithersburg, MD), and incubated at 37°C for 1 hr. Subsequently, two rounds of PCR amplification with nested primer pairs were performed; the template for the second PCR was 1 μl of the first reaction. The concentration of primers was 60 μM.

The large sequence diversity of K^+ channel subunits at the nucleotide level required the use of multiple sets of specific primers rather than a single set of degenerate primers. To exclude unpredictable primer interactions, the material from each neuron was amplified only with a single set of primers (requiring a large number of cells to be analyzed, $n = 100$). Transcripts of the Kv1 subfamily (Kv1.1 and Kv1.6, and Kv1.2 and Kv1.4, respectively), of the Kv2 subfamily (Kv2.1 and Kv2.2), and Kv4 subfamily (Kv4.1, Kv4.2, and Kv4.3) were amplified with common primers in the same two-step PCR. Control experiments showed that these primers amplified the respective cDNAs in plasmid mixtures with the same efficacy. Transcripts of the Kv3 subfamily (Kv3.1 and Kv3.2) were amplified with specific primers in different PCRs because attempts to employ common primers failed, resulting in unequal amplification of Kv3.1 and Kv3.2 in plasmid mixtures.

Primers in the two rounds of amplification were nested and intron-overspanning whenever possible. For all PCR reactions the cycle conditions were: 94°C for 5 min, after a hot start, 35 step cycles (94°C for 30 sec; 55°C for 30 sec; 72°C for 40 sec), and 72°C for 10 min. Positive controls for primer efficiency were run using plasmids. Controls for possible contamination artifacts were performed for each PCR amplification. Additional controls to exclude unspecific harvesting of surrounding tissue components were performed by advancing pipettes into the slice and taking them out again without seal formation and suction (Monyer and Jonas, 1995). Both types of controls gave negative results throughout. Amplification of genomic Kv2, Kv3, and Kv4 subunit DNA could be excluded by the intron-overspanning location of the primers. For Kv1 subunits, additional controls in which the RT was omitted were performed. Such controls were always negative only when the nucleus was not harvested. Thus, for Kv1 RT-PCR the nucleus was never aspirated, even if this resulted in a lower amount of cytoplasm collected. To verify the specificity of the amplifications, the PCR products were tested using Southern blotting with radiolabeled oligonucleotides. The molecular identity of randomly selected PCR products was confirmed by sequencing.

Primer sequences and locations (referring to published sequences in the GenBank of the National Center for Biotechnology Information, www2.ncbi.nlm.nih.gov) were as follows: Kv1.1 (accession number M26161) and Kv1.6 (X17621): Upper primer, 5′-TGG TGA TCA ACA TCT C(CT)G GGC-3′ (position 150–170 and 558–578, respectively); upper nested primer, 5′-ATC CTT TAT TAC TAC CAG TCG G-3′ (308–329, 716–737); lower primer, 5′-GTC TCC AGG CAA AAG ATG AC-3′ (578–597, 995–1014). Kv1.2 (X16003) and Kv1.4 (X16002): Upper primer, 5′-AGC TTT GAT GCC ATT TTG TA-3′ (812–831, 1176–1195); upper nested primer, 5′-ACA G(GA)T (GT)TG GCT TCT CTT TGA ATA-3′ (1003–1026, 1370–1393); lower primer, 5′-AGA GGA TGA CCC C(AG)A TGA AGA G-3′ (1565–1586, 1950–1971). Kv2.1 (X16476) and Kv2.2 (M77482): Upper primer, 5′-CTG GGG CAT CGA TGA GAT CTA CC-3′ (372–394, 701–723); lower primer, 5′-GTC ATG GTG ATG GTA GCC CAC CA-3′ (1104–1126, 1443–1465); lower nested primer, 5′-CGA AAG ATC TGG ACC ACG CG-3′ (889–908, 1218–1237). Kv3.1 (X62840): Upper primer, 5′-CAA GAG ATT GGC GCT CAG TGA C-3′ (742–763); lower primer, 5′-CCC AG(AG) GCC AG(AG) AAG ATG AT(AC) AGC A-3′ (1326–1350); lower nested primer, 5′-AA(AG) TGG CG(GT) GT(ACG) AGC TTG AAG AT-3′ (1247–1269). Kv3.2 (M59211): Upper primer, 5′-TTG AGG ATG CTG CGG GGC TGG-3′ (611–631); lower primer, same as for Kv3.1 (1187–1211); lower nested primer, same as for Kv3.1 (1108–1130). Kv4.1 (M64226), Kv4.2 (S64320), Kv4.3 (U75448): Upper primer, 5′-T(CT)A TCG A(TC)G TGG TGG CCA TC-3′ (797–816, 1342–1361, 802–821); upper nested primer, 5′-TAC AC(AC) CT(CG) AAG AGC TGT GC-3′ (943–962, 1494–1513, 954–973); lower primer, 5′-TGG TAG AT(CG) C(GT)(GA) CT(AG) AAG TT-3′ (1228–1247, 1773–1792, 1223–1242).

The sequences of the probes for the Southern blots were: Kv1.1, 5′-CTT CAT CAA GGA AGA GGA GCG CCC CCT A-3′ (439–466); Kv1.2, 5′-TGG TGG GGT GAC CTT CCA CAC CTA TTC-3′ (1153–1179); Kv1.4, 5′-CGC AGG TGG ACA CAG CAG ATT ATT GAA T-3′ (1526–1553); Kv1.6, 5′-TTG CCT GCC CGA AGG TGG TGA GGA TGA G-3′ (847–874); Kv2.1, 5′-CTC TGG CCG AAC TCG TCT AGG CTC-3′ (654–677); Kv2.2, 5′-GGT TGC CCA AAT TCA TCG TTT TCT-3′ (983–1006); Kv3.1, 5′-TGA GAA CGT TCG AAA TGG CAC AC-3′ (958–980); Kv3.2, 5′-CCA GTC ATC AAC GGC ACC AGC-3′ (823–843); Kv4.1, 5′-CTT GCC TGT GCC AGT CAT TGT A-3′ (1203–1224); Kv4.2, 5′-GCT ACC CGT GCC TGT GAT CGT G-3′ (1748–1769); Kv4.3, 5′-TCT GCC AGT CCC CGT CAT AGT C-3′ (1208–1229).

The washing conditions were 0.5× SSC at 55°C, except for Kv1 probes (0.2× SSC at 55°C) and Kv4.2 probes (0.1× SSC at 55°C).

RESULTS

Macroscopic K^+ currents differ between interneurons and principal neurons

BCs and PCs differ in the frequency of action potentials generated by sustained current injection (Fig. 1*A*,*B*), suggesting a possible difference in the functional properties of the voltage-gated K^+ channels expressed. We have therefore studied the somatic K^+ channels in these two types of neurons using the nucleated patch configuration, which allowed us to examine channel gating under almost ideal voltage-clamp conditions. Representative recordings of K^+ currents activated by test pulses to potentials between −80 and 70 mV are shown in Figure 1*C*,*D*.

The K^+ currents in the two classes of cells differed in the voltage dependence of activation. The normalized K^+ conductance–voltage relations, calculated from the respective peak current amplitudes, showed indistinguishable midpoint potentials ($p > 0.5$) but significantly steeper voltage dependence in BC patches than in PC patches (slope factors were $k = 17.6 \pm 0.7$ mV and 24.0 ± 0.3 mV, respectively; $p < 0.001$; Fig. 1*E*). Accordingly, the threshold for K^+ channel activation was ~10 mV more positive in BCs than in PCs (Fig. 1*E*).

K^+ currents in the two classes of neurons also differed markedly in the time course and the extent of inactivation. K^+ currents in BC patches showed only minimal inactivation during 100 msec pulses, whereas K^+ currents in PC patches decayed substantially (Fig. 1*C*,*D*). The ratio of the current at the end of a 100 msec pulse to 70 mV to that at the peak was on average 0.75 ± 0.02 for BCs ($n = 66$) and 0.35 ± 0.02 for PCs ($n = 44$, $p < 0.001$; Fig. 1*F*), independent of whether or not glutathione-SH (2 mM) was present in the internal solution (Ruppersberg et al., 1991).

In addition to these functional differences, the maximal value of the somatic K^+ conductance density differed between the two classes of neurons. For a test pulse to 70 mV and a K^+ current reversal potential of −95 mV (see Materials and Methods), the somatic K^+ conductance density was 175 pS μm^{-2} in BCs, significantly larger than in PCs (95 pS μm^{-2}; $p < 0.001$; Table 1). These results indicated that somatic macroscopic K^+ currents in the two types of neurons differed in several characteristics, such as voltage dependence of activation, time course of inactivation, and conductance density.

Dissection of three K^+ current components by external 4-AP and TEA

4-AP and TEA were shown previously to distinguish between recombinant K^+ channels assembled from subunits of different Kv subfamilies (Baldwin et al., 1991; Pak et al., 1991; Taglialatela et al., 1991; Rettig et al., 1992; Kirsch and Drewe, 1993). We, therefore, examined the effects of these blockers on the K^+ currents of the two cell types. Micromolar concentrations of external 4-AP, which selectively inhibit recombinant Kv3 channels (Kirsch and Drewe, 1993; Grissmer et al., 1994), reduced markedly the K^+ currents in BC patches (Fig. 2*A*) but had smaller effects in PC patches (Fig. 2*B*). The concentration dependence of the block by 4-AP is illustrated in Figure 2*C*. In both types of neurons, the data points could not be adequately fitted by a single Hill equation, independently of whether the Hill coefficient was constrained to 1 or left as a free parameter. We therefore fitted the data with the sum of two Hill equations, constraining the Hill coefficients to 1 (Kirsch and Drewe, 1993). The half-maximal inhibitory concentrations (IC_{50} values) of the two components were comparable in the two types of neurons (52 μM and 4.3 mM vs 15 μM and 1.8 mM), but their relative contribution was reverse. The high-affinity component predominated in BC patches, whereas the low-affinity component prevailed in PC patches (the blocked fractions were 69 and 20% vs 25 and 68%; Fig. 2*C*). These results indicated that the macroscopic K^+ current in both cell types consisted of multiple components that differed in their 4-AP sensitivity.

TEA blocks recombinant K^+ channels with very different affinities. Kv3 channels are highly sensitive to external TEA (Rettig et al., 1992), whereas Kv2 channels show intermediate sensitivity (Taglialatela et al., 1991), and Kv4 channels are TEA-resistant (Pak et al., 1991). External TEA reduced markedly the K^+ currents in BC patches (Fig. 2*D*) but had much smaller effects in PC patches (Fig. 2*E*). The concentration dependence of the block by TEA is depicted in Figure 2*F*. As with 4-AP, the sum of two Hill equations was required to fit adequately the data points. The IC_{50} values of the two components were 70 μM and 1.3 mM for BC patches and 10 μM and 1.7 mM for PC patches. The blocked fractions were substantially larger in BC patches than in PC patches (46 and 27% vs 6 and 25%; Fig. 2*F*). As with 4-AP, these results suggested that the K^+ current in both cell types consisted of two components with different TEA sensitivity, and a third, TEA-resistant component (Fig. 2*F*).

We next examined possible additive effects of low concentrations of 4-AP and TEA. In the presence of 0.5 mM 4-AP, further

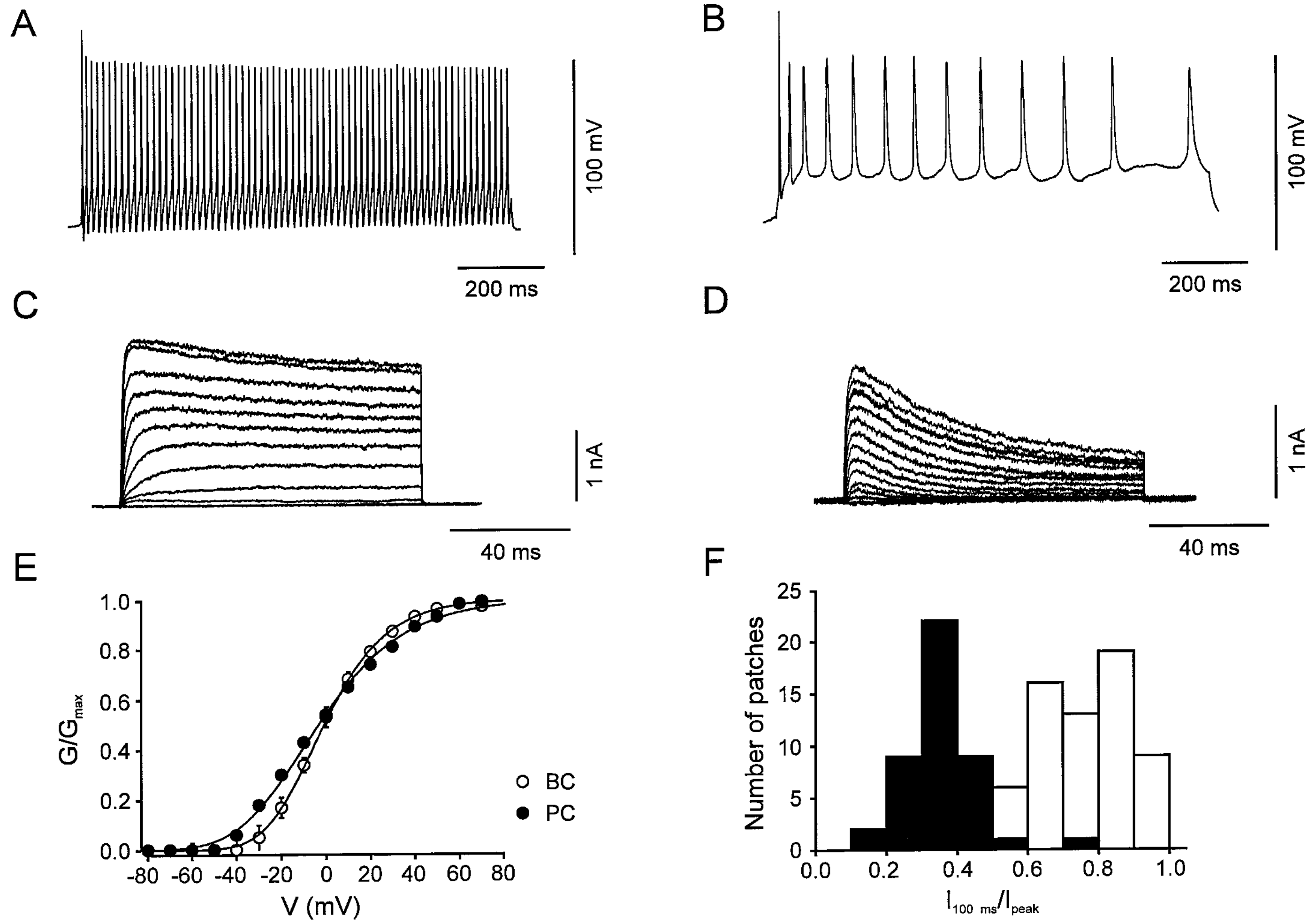

Figure 1. Interneurons and pyramidal neurons differ in action potential pattern and in activation and inactivation properties of their voltage-gated K$^+$ channels. *A*, *B*, Action potentials evoked by a 1 sec depolarizing current pulse in a BC (*A*) and a PC (*B*). Current-clamp recording in the whole-cell configuration. Membrane potential before the pulse was −70 mV. Current during the pulse was 160 and 120 pA, and holding current was −40 and −30 pA, respectively. One hundred micromolar Cd^{2+} was used in the external solution in both cell types. *C*, *D*, Traces of K$^+$ currents evoked in a nucleated patch isolated from a BC (*C*) and a PC (*D*); holding potential was −90 mV, pulse potential varied from −80 to 70 mV (10 mV increment). *E*, Peak conductance–voltage relation in nucleated patches isolated from BCs (*open circles*, $n = 25$) and PCs (*filled circles*, $n = 20$). The curves represent Boltzmann functions raised to the fourth power fitted to the data points. Midpoint potentials were −1.0 ± 1.2 mV in BC patches and −3.5 ± 1.5 mV in PC patches, and slope factors were 17.6 ± 0.7 mV and 24.0 ± 0.3 mV, respectively. *F*, Histogram of the ratio of current amplitude at the end of a 100 msec pulse to that of the peak current for 66 BC patches (*open bars*) and 44 PC patches (*filled bars*). For BC patches, the mean current ratio was 0.75 both in the presence ($n = 51$) and in the absence of glutathione-SH ($n = 15$). For PC patches, the mean current ratio was 0.35 in the presence ($n = 40$) and 0.39 in the absence of glutathione-SH ($n = 4$). Test pulse to 70 mV.

addition of 1 mM TEA reduced the peak K$^+$ current to 75 ± 2% in BC patches ($n = 4$) and 95 ± 6% in PC patches ($n = 5$). These effects were significantly smaller than those of 1 mM TEA in isolation ($p < 0.01$ for both cell types; Fig. 2*F*). Conversely, in the presence of 1 mM TEA, further addition of 0.2 mM 4-AP had no significant effect; the peak K$^+$ current was reduced to only 91 ± 3% and 94 ± 3% of the value in the presence of 1 mM TEA alone, respectively ($n = 3$, $p > 0.1$ in both cell types). These results indicated that the current that was highly sensitive to 4-AP was also highly sensitive to TEA and vice versa.

DTX (200 nM), a selective blocker of recombinant K$^+$ channels assembled from Kv1.1, Kv1.2, and Kv1.6 subunits (Pongs, 1992), had only minimal effects on the K$^+$ currents in both types of neurons; the peak current in the presence of DTX was 100.0 ± 2.0% of the control value in BC patches ($n = 6$, $p > 0.5$) and 95.0 ± 3.0% in PC patches ($n = 4$, $p > 0.01$; Fig. 2*G*,*H*).

Pharmacological dissection allowed us to separate the K$^+$ current components in the two types of neurons and to investigate their gating properties in isolation. Subtraction of currents evoked in the presence of low concentrations of either 4-AP (Fig. 3*A*,*B*, *top traces*) or TEA (Fig. 3*A*,*B*, *bottom traces*) from those in the absence of blockers revealed a first K$^+$ current component that showed fast activation and very little, if any, inactivation during 100 msec pulses. The 20–80% rise time was 0.9 ± 0.1 msec in BC patches ($n = 9$) and 1.5 ± 0.4 msec in PC patches ($n = 9$) at 70 mV test pulse potential. In contrast, subtraction of currents in the presence of 20 mM TEA plus 0.5 mM 4-AP from those in the presence of 0.5 mM 4-AP alone (Fig. 3*C*,*D*, *top traces*) or subtraction of the currents in the presence of 20 mM TEA from those in the presence of 1 mM TEA (Fig. 3*C*,*D*, *bottom traces*) revealed a second component with slower activation. The rise time was 6.3 ± 1.3 msec in BC patches ($n = 9$) and 5.4 ± 0.9 msec in PC patches ($n = 9$) at 70 mV. Finally, a third component that persisted in the presence of 20 mM TEA showed rapid activation and inactivation

Table 1. Comparison of functional properties of K^+ current components in BC and PC patches

	BCs	PCs	p
Total peak conductance density	175 ± 11 pS μm^{-2}	95 ± 6 pS μm^{-2}	<0.001*
Fast delayed rectifier	58 ± 6%	12 ± 4%	<0.001*
	(33–72%)	(1–22%)	
Activation curve			
midpoint V	−7.1 ± 0.9 mV	−12.1 ± 1.2 mV	<0.005
k	11.5 ± 0.8 mV	10.0 ± 1.0 mV	>0.1
	(14)	(9)	
Slow delayed rectifier	26 ± 5%	27 ± 4%	>0.5
	(14–40%)	(16–42%)	
Activation curve			
midpoint V	3.3 ± 4.9 mV	−7.5 ± 5.8 mV	>0.05
k	17.3 ± 1.5 mV	26.3 ± 1.8 mV	<0.005
	(9)	(9)	
Inactivation curve			
midpoint V	−63.8 ± 6.2 mV	−70.0 ± 3.4 mV	>0.1
k	11.1 ± 2.0 mV	7.8 ± 1.7 mV	>0.5
noninact. comp.	(37 ± 5%)	(16 ± 2%)	>0.05
	(9)	(10)	
A-type	17 ± 4%	61 ± 4%	<0.001*
	(6–24%)	(52–84%)	
Activation curve			
midpoint V	−6.2 ± 3.3 mV	−3.0 ± 3.6 mV	>0.5
k	23.0 ± 0.7 mV	27.0 ± 0.5 mV	<0.05
	(9)	(11)	
Inactivation curve			
midpoint V	−75.5 ± 2.5 mV	−77.3 ± 3.2 mV	>0.5
k	8.5 ± 0.8 mV	7.4 ± 0.4 mV	>0.5
	(9)	(17)	
τ recovery from inactivation	30.1 ± 6.4 msec	22.8 ± 2.7 msec	>0.1
	(22 ± 4%)	(64 ± 3%)	<0.001*
	165 ± 49 msec	314 ± 80 msec	>0.1
	(55 ± 5%)	(16 ± 3%)	<0.001*
	(5)	(6)	

Values indicate mean, SEM, and total number of nucleated patches (in parentheses). Highly significant differences between BCs and PCs are indicated by asterisks. Activation curves were fitted with Boltzmann equations raised to fourth power, and inactivation curves were fitted with simple Boltzmann functions.

(Fig. 3*E*,*F*). The rise times were 0.9 ± 0.3 msec in BC patches and 1.0 ± 0.1 msec in PC patches, and the inactivation time constants were 43.8 ± 4.4 msec (n = 9) and 44.4 ± 4.5 msec (n = 11) at 70 mV test pulse potential, respectively.

These results indicated that the K^+ currents in both BCs and PCs were composed of three pharmacologically and kinetically distinct components: a fast delayed rectifier component that was highly sensitive to both 4-AP and TEA, a slow delayed rectifier with intermediate TEA-sensitivity, and an inactivating (A-type) K^+ current component that was largely TEA-resistant. The contribution of the three components to the total K^+ current, as assessed by subtraction analysis, differed substantially in the two types of neurons (Table 1). In BC patches, the relative contributions of the three components were 58 ± 6%, 26 ± 5%, and 17 ± 4%. In contrast, in PC patches the contributions were 12 ± 4%, 27 ± 4%, and 61 ± 4% (Table 1).

Activation and inactivation of the three K^+ current components

We next compared the voltage dependence of activation and inactivation of the three pharmacologically dissected current components in BC and PC patches. The fast delayed rectifier component in BC patches showed an activation curve with a midpoint potential of −7.1 ± 0.9 mV and steep activation characteristics (slope factor k = 11.5 ± 0.8 mV; Fig. 4*A*,*C*; Table 1). This component showed no inactivation during 100 msec pulses and very little inactivation by 10 sec prepulses (Fig. 4*B*,*D*). The 20–80% rise time was strongly voltage-dependent, ranging from 16.8 msec at −10 mV to 0.9 msec at 70 mV (Fig. 4*E*). A striking kinetic property was the very fast deactivation kinetics; the deactivation time constant at −40 mV was on average 5.8 ± 0.4 msec (n = 8; Fig. 4*F*). The corresponding K^+ current component in PC patches was similar (Fig. 4); the only significant difference between the two cell types was the more negative midpoint potential of the activation curve in PCs (Table 1).

The slow delayed rectifier component in BC patches showed an activation curve with more positive midpoint potential (3.3 ± 4.9 mV) and less steep voltage dependence (slope factor, 17.3 ± 1.5 mV; Fig. 5*A*,*C*; Table 1) than that of the fast delayed rectifier component. This K^+ current showed little inactivation during 100 msec test pulses but substantial inactivation by 10 sec prepulses

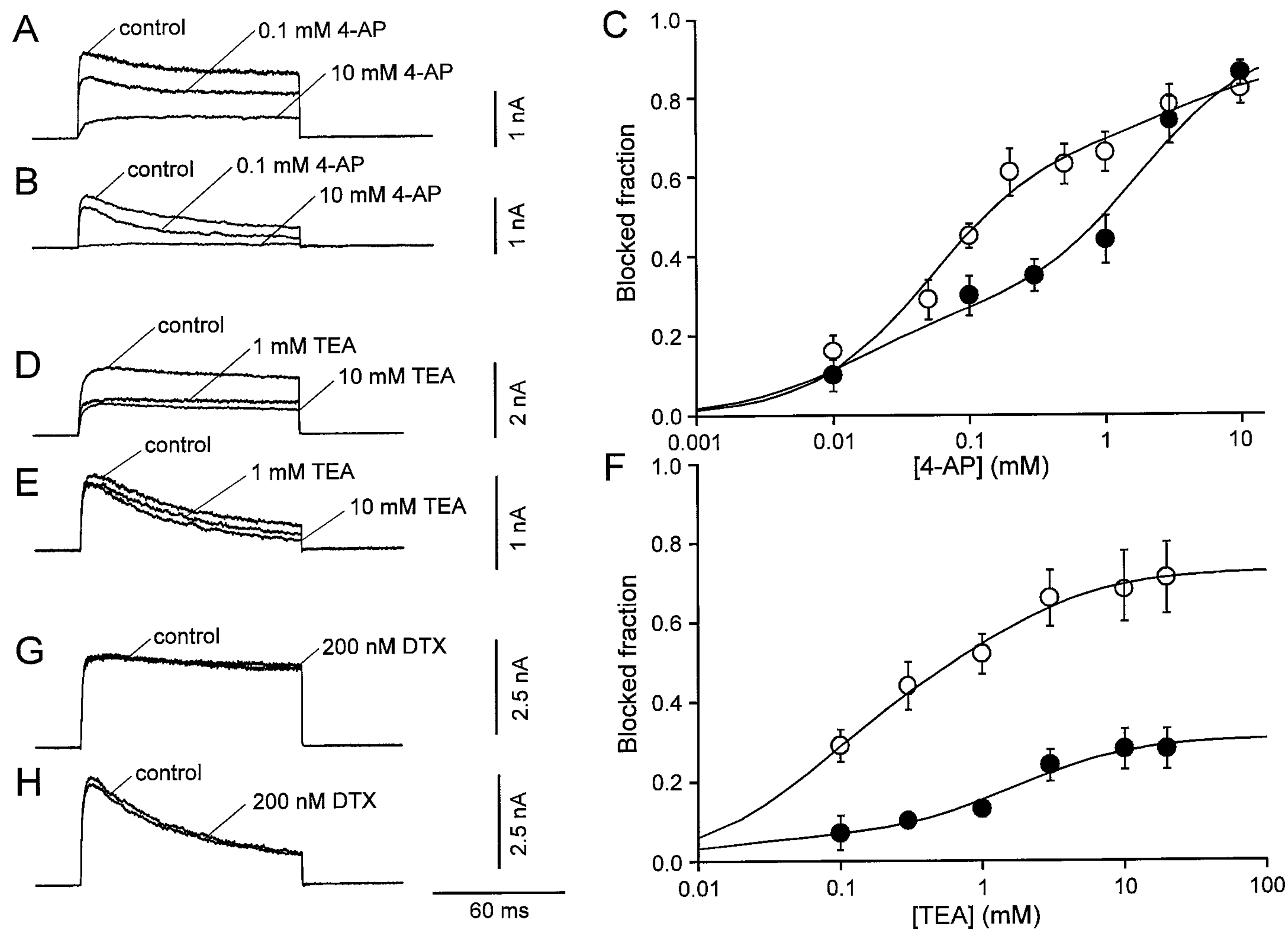

Figure 2. Effects of external 4-AP, TEA, and DTX on K^+ current components in interneurons and pyramidal neurons. *A*, *B*, K^+ currents evoked by test pulses to 70 mV (from a holding potential of −90 mV) in the absence and in the presence of 0.1 and 10 mM 4-AP in a BC patch (*A*) and a PC patch (*B*). *C*, Inhibition of the peak K^+ current by 4-AP, plotted against 4-AP concentration, for BC patches (*open circles*, $n = 6$) and PC patches (*filled circles*, $n = 5$). Data points were fitted with the sum of two Hill equations. For BC patches, the IC_{50} values were 52 μM and 4.3 mM, and the blocked fractions were 69 and 20%. For PC patches, the IC_{50} values were 15 μM and 1.8 mM, and the blocked fractions were 25 and 68%, respectively. *D*, *E*, K^+ currents evoked by test pulses to 70 mV (from a holding potential of −90 mV) in the absence and in the presence of 1 or 10 mM TEA in a BC patch (*D*) and a PC patch (*E*). *F*, Inhibition of the peak K^+ current by TEA, plotted against TEA concentration, for BC patches (*open circles*, $n = 8$–22) and PC patches (*filled circles*, $n = 6$–10). Data points were fitted with the sum of two Hill equations. For BC patches, the IC_{50} values were 70 μM and 1.3 mM, and the blocked fractions were 46 and 27%. For PC patches, the IC_{50} values were 10 μM and 1.7 mM, and the blocked fractions were 6 and 25%, respectively. The Hill coefficients were constrained to 1 in all cases. *G*, *H*, DTX (200 nM) had only minimal effects on the K^+ current in BC patches (*G*) and PC patches (*H*).

(Fig. 5*B*,*D*). In agreement with the less steep activation curve, the rise time was less voltage-dependent, ranging from 14.3 msec at −10 mV to 6.4 msec at 70 mV (Fig. 5*E*). The deactivation kinetics were markedly slower than those of the first component; the deactivation time constant at −40 mV was on average 22.3 ± 2.0 msec ($n = 6$; Fig. 5*F*). The slow delayed rectifier K^+ current component in PC patches was similar to that in BC patches in some but not all functional properties. Significant differences between the two classes of cells were found in the steepness of the activation curves (Fig. 5*C*, Table 1) and in the rise times of the current for potentials ≤20 mV (Fig. 5*E*; $p < 0.01$ at −10 mV).

The A-type, TEA-insensitive, component in BC patches had an activation curve with a midpoint potential of −6.2 ± 3.3 mV and a slope factor of 23.0 ± 0.7 mV (Fig. 6*A*,*C*; Table 1). The current component showed marked inactivation during 100 msec test pulses and complete inactivation by 10 sec prepulses. The steady-state inactivation curve had a midpoint potential of −75.5 ± 2.5 mV and showed steep voltage dependence (slope factor, 8.5 ± 0.8 mV; Fig. 6*B*,*D*). Both the rise time of the current and the time constant of inactivation onset were fast and largely independent of voltage (Fig. 6*E*,*F*).

The A-type K^+ current component in PC patches was indistinguishable from that in BC patches in all functional properties examined, except in the kinetics of the recovery from inactivation. The inactivation recovery time course, investigated by a double-pulse protocol, was biexponential in both classes of cells. However, the slow component predominated in BC patches, whereas the fast component prevailed in PC patches. In contrast, the values of the time constants were similar in the two classes of neurons (Fig. 6*G*,*H*; Table 1).

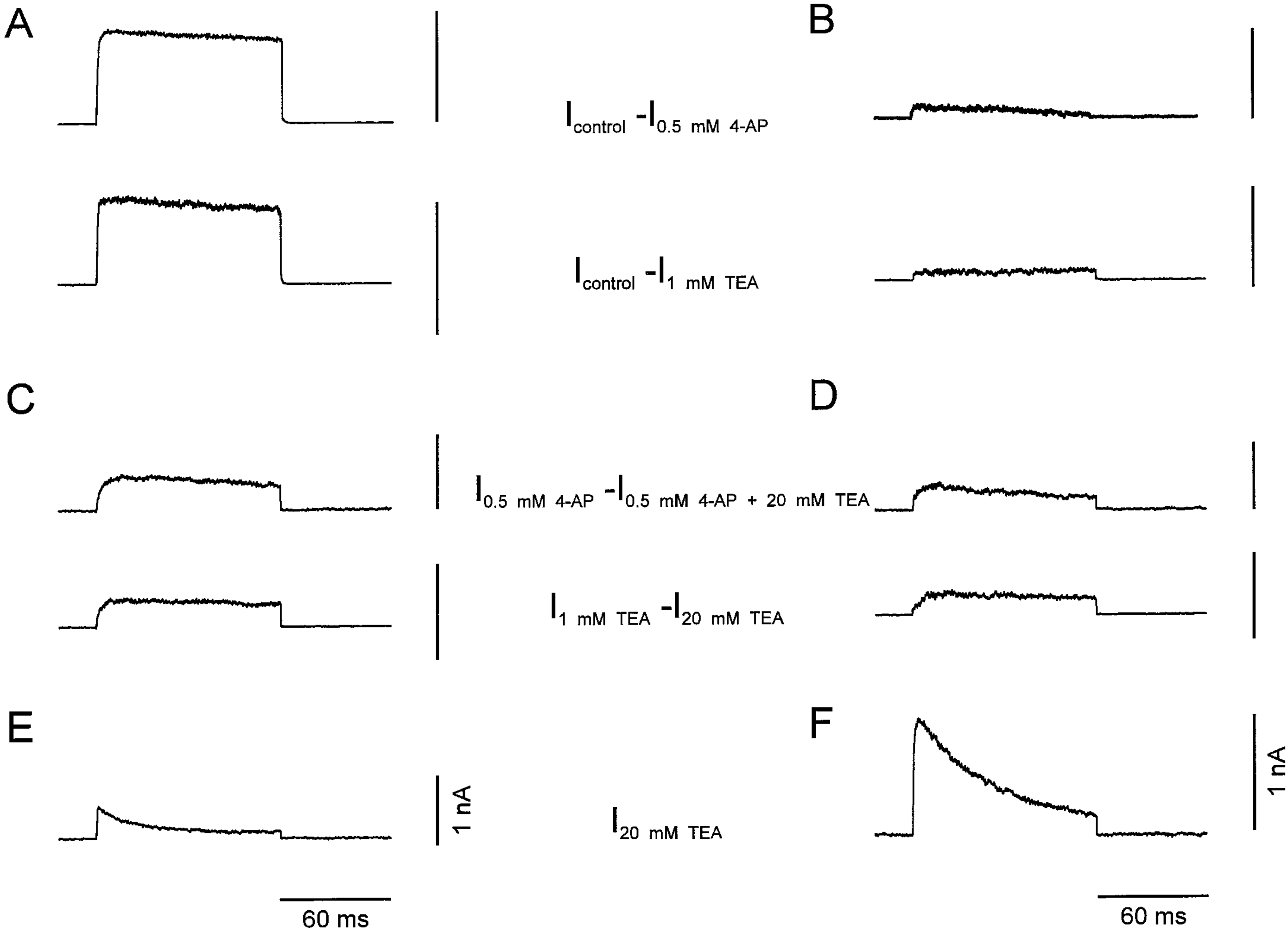

Figure 3. Current subtraction analysis suggests the presence of three kinetically distinct K^+ current components. *A*, *B*, Fast delayed rectifier K^+ current component, $I_{\mathrm{control}} - I_{0.5\ \mathrm{mM}\ 4\text{-}\mathrm{AP}}$ (*top traces*) or $I_{\mathrm{control}} - I_{1\ \mathrm{mM}\ \mathrm{TEA}}$ (*bottom traces*). *C*, *D*, Slow delayed rectifier K^+ current component, $I_{0.5\ \mathrm{mM}\ 4\text{-}\mathrm{AP}} - I_{0.5\ \mathrm{mM}\ 4\text{-}\mathrm{AP}\ +\ 20\ \mathrm{mM}\ \mathrm{TEA}}$ (*top traces*) or $I_{1\ \mathrm{mM}\ \mathrm{TEA}} - I_{20\ \mathrm{mM}\ \mathrm{TEA}}$ (*bottom traces*). *E*, *F*, A-type K^+ current component, $I_{20\ \mathrm{mM}\ \mathrm{TEA}}$. Traces in *A*, *C*, and *E* were recorded from BC patches, traces in *B*, *D*, and *F* from PC patches. Currents were evoked by test pulses to 70 mV (from a holding potential of −90 mV).

Single-cell RT-PCR analysis of K^+ channel subunit transcripts

A comparison of the functional properties of K^+ channels in BC and PC patches with those of recombinant K^+ channels (Baldwin et al., 1991; Pak et al., 1991; Taglialatela et al., 1991; Rettig et al., 1992; Grissmer et al., 1994) may suggest that the fast delayed rectifier K^+ current component that predominated in BCs was mediated by Kv3 subunits, whereas the inactivating component that predominated in PCs was mediated by Kv4 subunits. According to the functional properties, the slow delayed rectifier component could be attributable to Kv2 subunits, but the contribution of Kv1 subunits could not be excluded entirely. We therefore analyzed the expression of Kv1, Kv2, Kv3, and Kv4 subunit transcripts by single-cell RT-PCR. The cytoplasm of single neurons was harvested into the recording pipette, and the harvested material was used for reverse transcription and PCR with specific nucleotide primers (Monyer and Jonas, 1995; see Materials and Methods). The amplified cDNA products were visualized on ethidium bromide-stained gels and probed with specific radiolabeled oligonucleotides (Fig. 7).

Single-cell RT-PCR analysis revealed that Kv1, Kv2, Kv3, and Kv4 subunits were expressed differentially in BCs and PCs (Figs. 7, 8). The Kv3.1 subunit mRNA was detected in 89% of BCs (n = 9) but only in 17% of PCs examined (n = 6). Similarly, 83% of BCs expressed Kv3.2 subunit mRNA (n = 6), whereas only 17% of PCs were Kv3.2 mRNA-positive (n = 6). In contrast, the Kv4 subunit mRNA was the dominant Kv mRNA species in pyramidal neurons; it was detected in 87% of PCs (n = 15) but also in 55% of BCs analyzed (n = 11; Figs. 7, 8). The Kv2 subunit mRNA was detected in 31% of BCs (n = 13) and in 67% of PCs (n = 12), suggesting that subunits from this subfamily were the major contributors to the slow delayed rectifier component in both types of neurons. Kv1 subunit mRNA levels were low in both cell types. With Kv1.1/Kv1.6 common primers, 33% of BCs (n = 6) and 20% of PCs (n = 5) were positive; with Kv1.2/Kv1.4 common primers, 0% of BCs (n = 5) and 33% of PCs (n = 6) were positive.

Southern blot analysis confirmed the identity of the PCR products and, in addition, revealed that multiple mRNA members of a given Kv subfamily were frequently coexpressed in a single cell. For the Kv4 subfamily, 18% of BCs expressed both Kv4.2 and Kv4.3 mRNA, 27% were positive only for Kv4.2 mRNA, and 9% were positive only for Kv4.3 mRNA. In 46% of PCs both Kv4.2

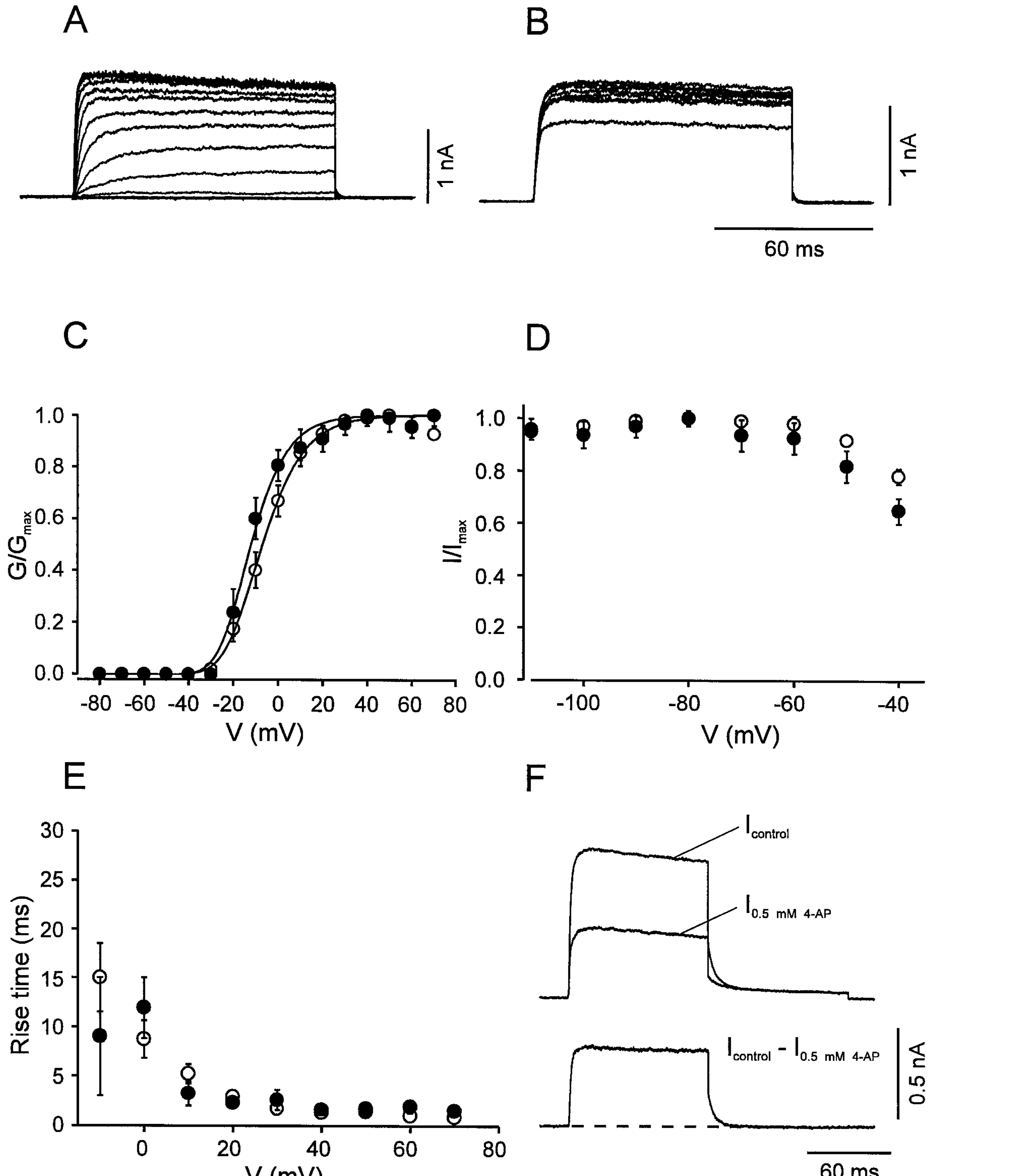

Figure 4. Activation and inactivation of the fast delayed rectifier K^+ current component. *A*, *B*, Traces of K^+ current obtained by subtraction ($I_{control} - I_{0.5\ mM\ 4\text{-}AP}$) in BC patches. In *A*, the test pulse potential was varied from −80 to 70 mV (10 mV increment), and the holding potential was −90 mV. In *B*, the potential of the prepulse (10 sec) was varied from −110 to −40 mV, and the test pulse potential was kept constant at 20 mV. *C*, Activation curves for BC patches (*open circles*, $n = 14$) and PC patches (*filled circles*, $n = 9$). Data points were fitted with Boltzmann functions raised to the fourth power. Pulse program as described in *A*. *D*, Steady-state inactivation curves for BC patches (*open circles*, $n = 6$) and PC patches (*filled circles*, $n = 5$). Pulse program as described in *B*. *E*, 20–80% rise time, plotted against test pulse voltage for BC patches (*open circles*, $n = 14$) and PC patches (*filled circles*, $n = 9$). Data in *C–E* were obtained by subtraction of either $I_{control} - I_{0.5\ mM\ 4\text{-}AP}$ or $I_{control} - I_{1\ mM\ TEA}$. Because the two approaches gave similar results, data were pooled. *F*, Deactivation time course at −40 mV in a BC patch. Pulse program: holding potential −90 mV, 100 msec pulse to 20 mV, 100 msec pulse to −40 mV, and step back to −90 mV. *Top traces* were obtained in the absence and presence of 0.5 mM 4-AP, *bottom trace* represents subtracted current. Note the fast deactivation of the 4-AP-sensitive component (decay τ 4.9 msec for the trace shown). For curve parameters, see Table 1.

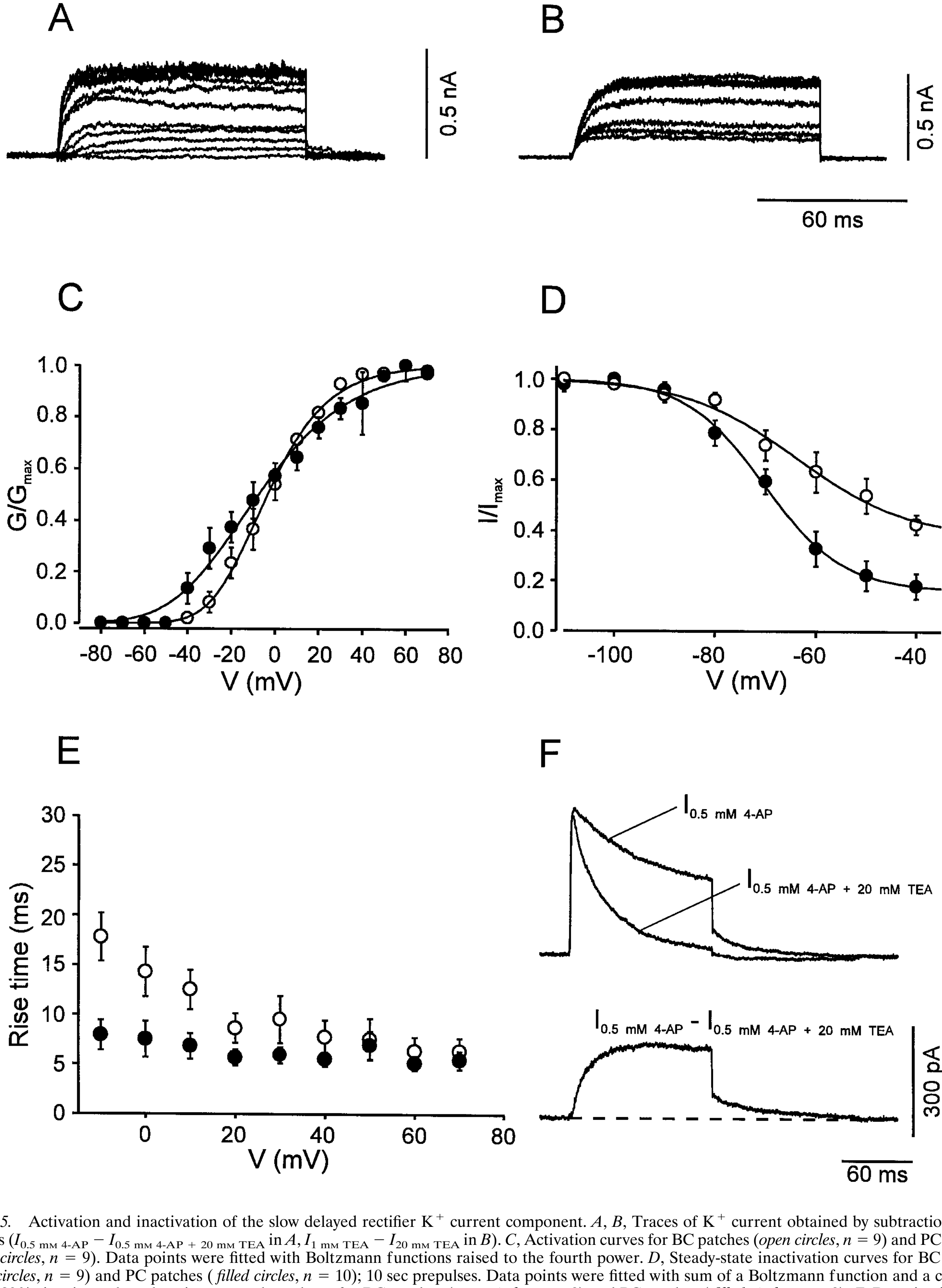

Figure 5. Activation and inactivation of the slow delayed rectifier K^+ current component. *A*, *B*, Traces of K^+ current obtained by subtraction in BC patches ($I_{0.5\ \mathrm{mM}\ 4\text{-AP}} - I_{0.5\ \mathrm{mM}\ 4\text{-AP}\ +\ 20\ \mathrm{mM}\ \mathrm{TEA}}$ in *A*, $I_{1\ \mathrm{mM}\ \mathrm{TEA}} - I_{20\ \mathrm{mM}\ \mathrm{TEA}}$ in *B*). *C*, Activation curves for BC patches (*open circles*, $n = 9$) and PC patches (*filled circles*, $n = 9$). Data points were fitted with Boltzmann functions raised to the fourth power. *D*, Steady-state inactivation curves for BC patches (*open circles*, $n = 9$) and PC patches (*filled circles*, $n = 10$); 10 sec prepulses. Data points were fitted with sum of a Boltzmann function and a constant. *E*, 20–80% rise time, plotted against test pulse voltage for BC patches (*open circles*, $n = 9$) and PC patches (*filled circles*, $n = 9$). *F*, Deactivation time course at −40 mV in a BC patch. *Top traces* represent $I_{0.5\ \mathrm{mM}\ 4\text{-AP}}$, and $I_{0.5\ \mathrm{mM}\ 4\text{-AP}\ +\ 20\ \mathrm{mM}\ \mathrm{TEA}}$, *bottom trace* represents subtracted current. Note the slow deactivation (decay τ 21.6 msec). Pulse programs identical to those used for Figure 4. For curve parameters, see Table 1.

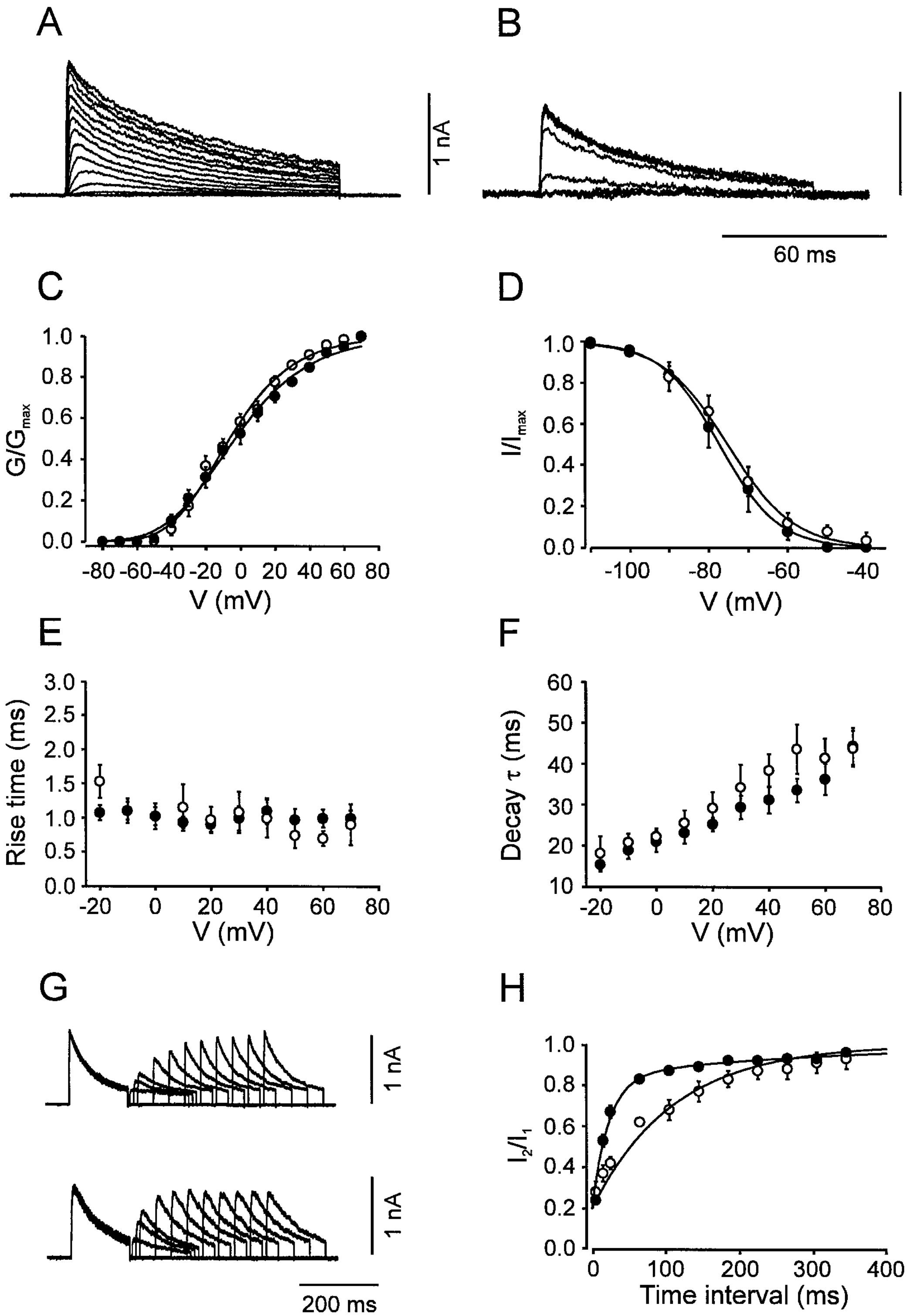

Figure 6. Activation and inactivation of the A-type K^+ current component. *A*, *B*, Traces of K^+ current in the presence of 20 mM TEA in BC patches. *C*, Activation curves for BC patches (*open circles*, $n = 9$) and PC patches (*filled circles*, $n = 11$). Data points were fitted with Boltzmann functions raised to the fourth power. *D*, Steady-state inactivation curves for BC patches (*open circles*, $n = 9$) and PC patches (*filled circles*, $n = 17$); 10 sec prepulses. Data points were fitted with Boltzmann functions. *E*, 20–80% rise time, plotted against test pulse voltage. *F*, Decay τ, plotted against test pulse voltage, for BC patches (*open circles*, $n = 9$) and PC patches (*filled circles*, $n = 11$). The decay phase of the current during a 100 msec pulse was fitted with the sum of a single exponential function and a constant. *G*, Traces of K^+ currents in the presence of 20 mM TEA. Pulse protocol: holding potential −90 mV, 150 msec pulse to 50 mV (conditioning pulse), pulse of variable duration to −90 mV, 150 msec pulse to 50 mV (test pulse), and step back to −90 mV. *Top traces* from a BC patch, *bottom traces* from PC patch. *H*, Time course of recovery from inactivation for BC patches (*open circles*, $n = 5$) and PC patches (*filled circles*, $n = 6$). The amplitude of the peak current evoked by the test pulse divided by that evoked by the conditioning pulse was plotted against the interpulse interval. Data points were fitted with the sum of two exponentials. Pulse programs in *A–F* were identical to those used for Figure 4. For curve parameters, see Table 1.

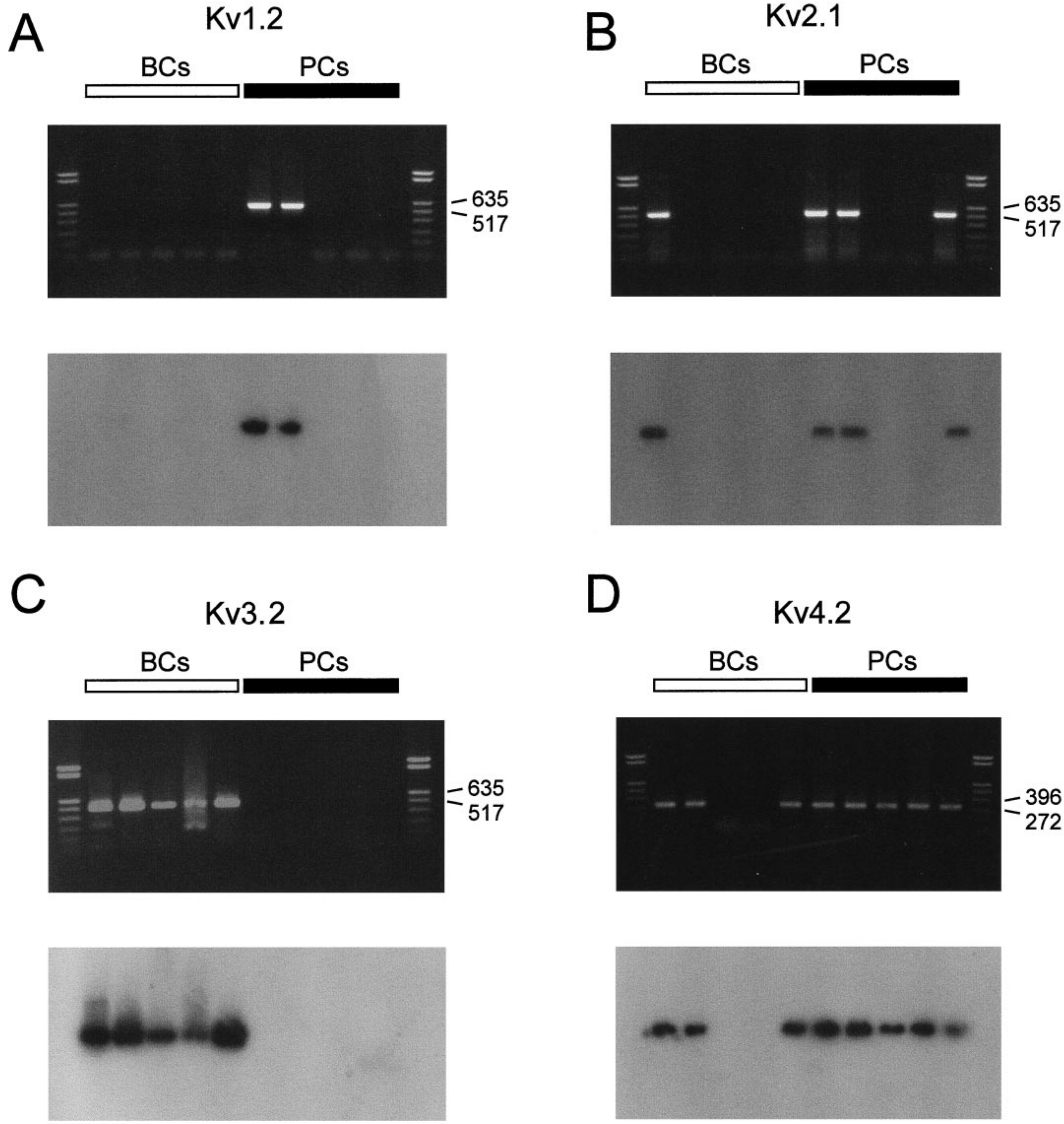

Figure 7. Differential expression of Kv1, Kv2, Kv3, and Kv4 subunit mRNAs in BCs and PCs. *Top panels*, ethidium bromide-stained gels of the PCR products amplified with primers specific for Kv1.2/Kv1.4 (*A*), Kv2.1/Kv2.2 (*B*), Kv3.2 (*C*), and Kv4.1/Kv4.2/Kv4.3 transcripts (*D*). *Bottom panels*, Differential hybridization of gels with selective radiolabeled oligonucleotide probes specific for Kv1.2 (*A*), Kv2.2 (*B*), Kv3.2 (*C*), and Kv4.2 transcripts (*D*). *Left lanes*, material from five different BCs; *right lanes*, from five different PCs. Molecular weight markers are shown in the lanes on the very left and right, together with the corresponding number of base pairs.

and Kv4.3 mRNA were detected, and 40% were positive only for Kv4.2 mRNA, whereas the exclusive expression of Kv4.3 mRNA was never observed. None of the cells expressed Kv4.1 subunit mRNA. For the Kv2 subfamily, 15% of BCs expressed both Kv2.1 and Kv2.2 mRNA, whereas 8% were positive for either Kv2.1 or Kv2.2 mRNA, respectively. Similarly, in 50% of PCs both Kv2.1 and Kv2.2 mRNA were detected, but only 8% were positive for either Kv2.1 or Kv2.2 mRNA. For the Kv1 family, 33% of BCs expressed Kv1.1 mRNA, whereas Kv1.2, Kv1.4, and Kv1.6 mRNA were not detected. In PCs, 20% of cells expressed Kv1.1 mRNA;

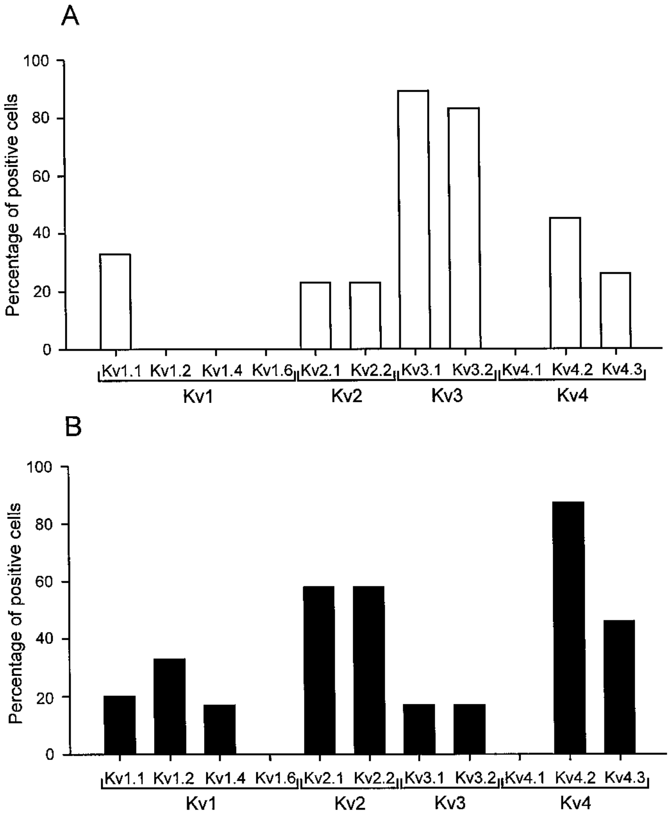

Figure 8. Expression profile of Kv1, Kv2, Kv3, and Kv4 subunit mRNAs in BCs and PCs. *A*, Percentage of BCs expressing a given K^+ channel subunit transcript; *B*, percentage of PCs expressing a given transcript. A cell was considered to express a given subunit mRNA when the ethidium bromide-stained gel showed a signal of the expected molecular weight, and the Southern blot with the respective oligonucleotide probe gave a positive result. A direct comparison of the values obtained for Kv1 to those for Kv2, Kv3, and Kv4 may not be possible because the harvesting procedure was different (see Materials and Methods).

17% of cells coexpressed Kv1.2 and Kv1.4 mRNA, whereas 17% were positive only for Kv1.2 mRNA. None of the cells expressed Kv1.6 subunit mRNA. These results showed a differential expression of K^+ channel subunit mRNAs between interneurons and pyramidal neurons and were consistent with the view that the K^+ channels in the two cell types were mainly assembled from Kv2, Kv3, and Kv4 subunits. In addition, the results indicate coexpression of mRNAs of multiple members of a subfamily in a single neuron, suggesting the possibility of the formation of heteromeric channels.

Selective activation of fast delayed rectifier K^+ channels during high-frequency action potential trains

The present results showed that fast delayed rectifier K^+ channels, probably assembled from Kv3 subunits, predominated in BCs. To examine directly the contribution of these channels to the fast-spiking phenotype, we investigated the effects of low concentrations of 4-AP on the action potential pattern of BCs (Fig. 9*A*,*B*). Application of 4-AP at a concentration that blocked the fast delayed rectifier K^+ current component selectively (0.2 mM) converted the fast-spiking phenotype into a substantially slower spiking mode (Fig. 9*B*; $n = 4$), indicating a main contribution of Kv3 channels in fast spiking.

To quantify the contribution of the three K^+ current components to repolarization and afterhyperpolarization during a high-frequency spike train, action potential patterns were applied as voltage-clamp commands to BC patches (Fig. 9*C*). The transient outward currents activated by each spike were almost completely blocked by 0.2 mM 4-AP ($n = 3$), indicating that the fast delayed rectifier K^+ channels were activated selectively. Fast activation at the action potential peak and fast deactivation at the resting potential appeared to be the key properties that underlie the selective activation of these channels during action potential trains (Fig. 9*D*). In contrast, the contribution of the slow delayed rectifier K^+ channels and the A-type K^+ channels was minimal, presumably because their activation was too slow, or because they were largely inactivated at the resting potential.

DISCUSSION

Using the nucleated patch configuration that allows us to investigate somatic ion channels under almost ideal voltage-clamp conditions (Martina and Jonas, 1997), we have examined the kinetic properties of K^+ channels of identified fast-spiking interneurons and regularly spiking pyramidal neurons in brain slices from 11- to 16-d-old rats. In both BCs and PCs two distinct delayed rectifier K^+ current components and an A-type K^+ current component were identified. Whereas the functional characteristics of the three components were relatively similar in the two types of neurons, the contribution to the total current in nucleated patches differed substantially. The fast delayed rectifier K^+ current predominated in BC patches, whereas the A-type component was mainly found in PC patches. The slow delayed rectifier K^+ current was present in both types of neurons (Table 1).

Using single-cell RT-PCR, the most sensitive method for mRNA detection, we have analyzed the expression of Kv subunit mRNAs in BCs and PCs. Based on their functional properties, Kv2, Kv3, and Kv4 were the primary candidate subunits from which the native somatic channels were likely to be assembled. A contribution of members of the Kv1 subfamily as homomers or in combination with β subunits (Sewing et al., 1996) was less likely because recombinant Kv1.1, Kv1.2, and Kv1.6 channels are highly sensitive to DTX (Stühmer et al., 1989; Pongs, 1992), and Kv1.4 channels show very slow recovery from inactivation (Ruppersberg et al., 1990). The results of the RT-PCR analysis were consistent with the view that the reciprocal expression of Kv3.1/Kv3.2 and Kv4.2/Kv4.3 subunits underlies the different relative contributions of the fast delayed rectifier component and the A-type component in the two types of neurons.

Comparison with recombinant K^+ channels

In agreement with the results of the molecular analysis, the native K^+ current components showed several functional similarities with recombinant K^+ channels assembled from Kv3, Kv2, and Kv4 subunits, respectively.

The fast delayed rectifier K^+ current component resembled recombinant Kv3.1 and Kv3.2 channels in most basic properties (Rettig et al., 1992; Kirsch and Drewe, 1993; Grissmer et al., 1994). Like the native K^+ current component, Kv3.1 and Kv3.2 channels are highly sensitive to both external TEA (IC_{50} 0.1–0.2 mM) and 4-AP (0.08 mM), activate and deactivate rapidly (deactivation time constant at −40 mV, ~3 msec), and show only minimal inactivation. However, the midpoint potential of the activation curve of recombinant Kv3 channels is more positive (6–19 mV), whereas the voltage dependence is similar (6–10 mV

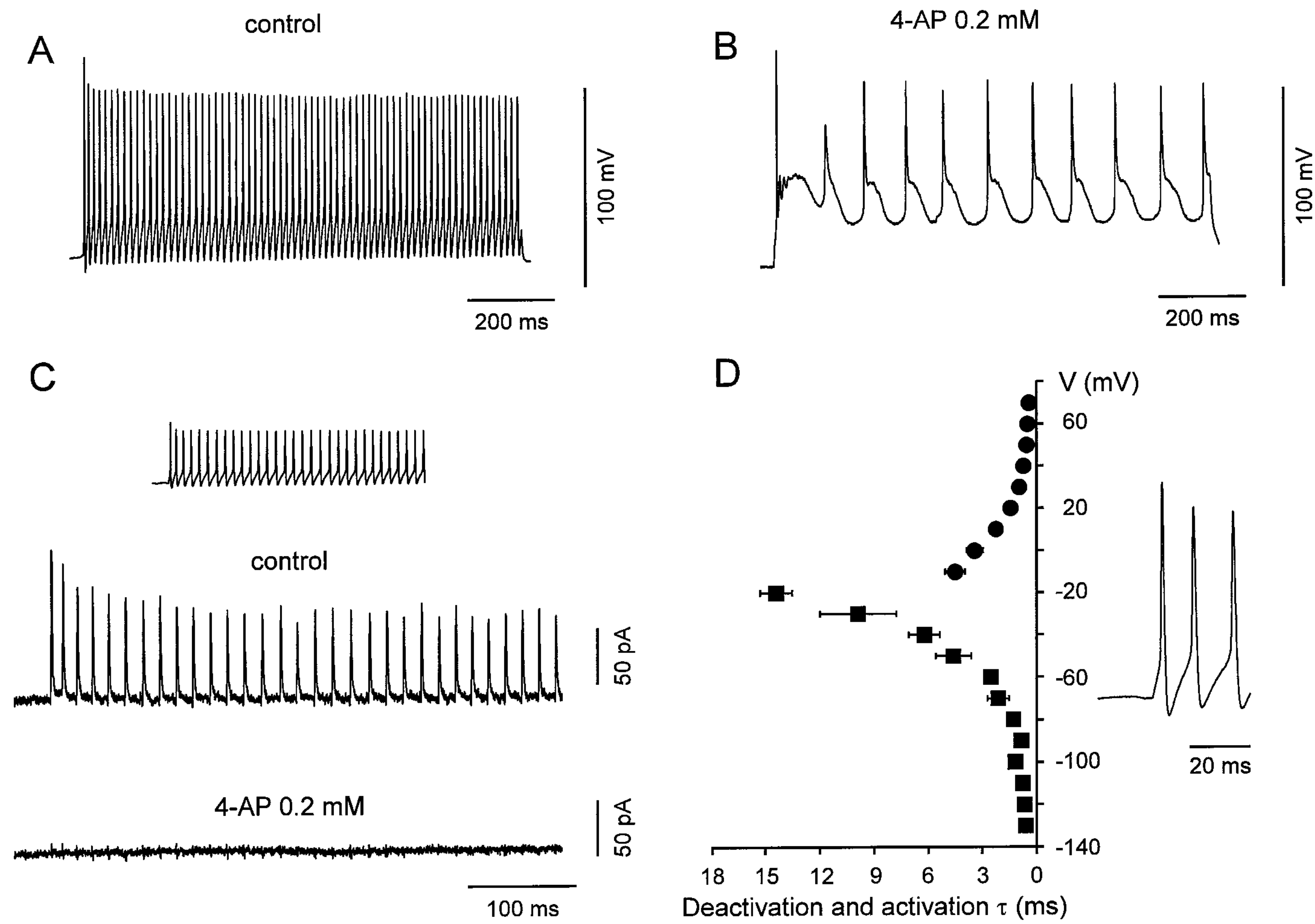

Figure 9. Kv3-type channels are the main voltage-gated K^+ channels contributing to the fast repolarizations and afterhyperpolarizations during action potential trains in BCs. *A*, *B*, Train of action potentials evoked in a BC (whole-cell, current-clamp recording) by a current pulse (1 sec, 160 pA), in the absence (*A*) and presence (*B*) of 0.2 mM 4-AP. Membrane potential before the pulse was −70 mV (holding current, −40 pA). One hundred micromolar Cd^{2+} was used in the external solution in both conditions. *C*, K^+ current in a BC patch during a high frequency train. The experimentally recorded action potential pattern was applied as voltage-clamp command (*inset*). The resulting current is shown in the absence (*top trace*) and presence (*bottom trace*) of 0.2 mM 4-AP, with 0.3 μM TTX added to the bath solution. Average of 10 individual sweeps, leak and capacitive currents were subtracted by a P over −4 procedure. Holding potential, −70 mV. Different BCs in *A*, *B*, and *C*. *D*, Summary graph of deactivation and activation time constants of the Kv3-like K^+ current component in BCs plotted against voltage. The voltage trajectories of BC action potentials are shown on the right.

voltage per e-fold change in conductance) to that observed for the native channels.

The slow delayed rectifier K^+ current component was similar to recombinant Kv2 channels in some but not all functional properties. Like the native K^+ current component, recombinant Kv2 channels show intermediate TEA-sensitivity (5.5 mM for recombinant Kv2 channels; Taglialatela et al., 1991) and slow activation time course. Unlike the native K^+ current, however, the midpoint potential of the inactivation curve of Kv2 channels is more positive (midpoint potential −25 mV; Shi et al., 1994).

The native A-type K^+ current component was very similar to recombinant Kv4 channels. Kv4 channels are insensitive to TEA (10 mM), are blocked only by high concentrations of 4-AP, and have a relatively flat activation curve (midpoint potential, −7 mV; slope factor, 20–22 mV; Baldwin et al., 1991; Pak et al., 1991). The midpoint potential and steepness of the inactivation curve (−69 and 4.7 mV; Pak et al., 1991) are also comparable to those of the native A-type K^+ current component. A contribution of Kv1.4 to the A-type current in BC and PC patches appeared unlikely, because the recovery of recombinant Kv1.4 channels from inactivation extends over several seconds (Ruppersberg et al., 1990).

DTX, a selective blocker of Kv1.1, Kv1.2, and Kv1.6 channels (Stühmer et al., 1989; Pongs, 1992), had only minimal effects on the K^+ current in both BC and PC patches, indicating that Kv1.1, Kv1.2, and Kv1.6 channels were not present at the soma of these neurons. Single-cell RT-PCR analysis revealed, however, that Kv1.1 is expressed in subsets of both BCs and PCs and that Kv1.2 is present in a subset of PCs. These results agree with previous *in situ* hybridization studies (Kues and Wunder, 1992) and may confirm the suggestion that Kv1 subunit proteins are specifically segregated to axons and presynaptic structures (Jonas et al., 1989; Sheng et al., 1994).

Differential expression of K^+ channel subunits in BCs and PCs

Previous studies indicated that Kv3.1 subunits are expressed preferentially in parvalbumin-positive, probably fast-spiking, interneurons in the hippocampus (Weiser et al., 1995; Du et al., 1996) and in fast-spiking interneurons of the neocortex (Massengill et al., 1997). Using single-cell RT-PCR analysis for several K^+ channel subunits, we extend these findings and show that both Kv3.1 and Kv3.2 subunit mRNA were expressed in almost all BCs, whereas they were detected only in a minor subset of PCs. Conversely, Kv4.2 and Kv4.3 subunit mRNAs were expressed in the majority of PCs, whereas the detection frequency in BCs was substantially lower. This suggests that the expression of Kv3 and Kv4 subunit genes in the two types of neurons is regulated reciprocally. Differential expression of Kv3 and Kv4 subunits appears to be part of a complex genetic program that regulates the expression of voltage- and ligand-gated ion channel subunits in both types of neurons (Geiger et al., 1995; Gan et al., 1996).

The present results indicate that the coexpression of multiple members of the same K^+ channel subfamily in a single cell is a main principle of the molecular organization of native K^+ channel mosaics. Evidence for coexpression is provided by the high percentage of interneurons positive for Kv3.1 and Kv3.2 mRNA (>80%) in RT-PCR experiments with specific primers and by the codetection of Kv2.1/Kv2.2, Kv4.2/Kv4.3, and Kv1.2/Kv1.4 subunit mRNA in experiments with common primers. This suggests that the macroscopic K^+ current in BCs and PCs could be mediated by heteromeric channels assembled independently from subunits of the different subfamilies (Ruppersberg et al., 1990; Covarrubias et al., 1991).

The coexpression of Kv3.1 and Kv3.2 subunits distinguishes dentate gyrus basket cells from several other neuron types that express the two subunits in an alternative manner (Weiser et al., 1994). Because the gating properties of recombinant Kv3.1 and Kv3.2 channels are almost indistinguishable, coexpression is unlikely to have direct impact on K^+ channel gating (Rettig et al., 1992). However, coexpression possibly enables specific regulatory pathways, because Kv3.2 (but not Kv3.1) subunits are inhibited by cAMP-dependent phosphorylation (Moreno et al., 1995). In addition, coexpression of Kv3.1 and Kv3.2 subunits provides a molecular backup system in interneurons that could compensate genetic K^+ channel defects. This may explain why Kv3.1-deficient mice unexpectedly do not show increased spontaneous seizure activity (Ho et al., 1997).

Functionally distinct K^+ channels shape the action potential patterns of central neurons

The present results indicate that the fast delayed rectifier K^+ channels, most likely assembled from Kv3.1 and Kv3.2 subunits, are the main channels contributing to the repolarization and afterhyperpolarization during action potential trains in fast-spiking hippocampal interneurons (Fig. 9). High voltage-activating Kv3 channels appear to be specialized to facilitate fast spiking because they limit action potential duration without affecting spike initiation (Kanemasa et al., 1995). The positive threshold and the steep voltage dependence of activation allow Kv3 channels to activate very quickly in the overshooting phase of an action potential. Once repolarization is completed, however, rapid deactivation of Kv3 channels ensures that the next spike can be generated with minimal delay.

The main function of A-type K^+ channels, presumably assembled from Kv4.2 and Kv4.3 subunits, appears to be facilitation of regular spiking with low frequency, contrary to that of Kv3 channels. Kv4 channels activate in the subthreshold voltage range and inactivate subsequently, thus delaying the initiation of action potentials (Hille, 1992; Song et al., 1998). The afterhyperpolarization after the spike then promotes recovery of Kv4 channels from inactivation, resetting them into the initial state. The location of the inactivation curve of these channels, however, indicates that they are partially inactivated at rest, particularly in interneurons that have more depolarized resting potentials than principal neurons (Scharfman, 1995). Thus, either hyperpolarization after activation of inhibitory synapses or synaptic release of modulatory substances (e.g., Zn^{2+} ions) is required to increase the number of available Kv4 channels (Talukder and Harrison, 1995).

In conclusion, the fast-spiking phenotype of basket cells in the dentate gyrus appears to be shaped by three main determinants that act in a synergistic manner: specific functional properties of interneuron Na^+ channels (steep steady-state inactivation curve and fast recovery from inactivation; Martina and Jonas, 1997), high level of expression of fast delayed rectifier K^+ channels assembled from Kv3.1 and Kv3.2 subunits, and low level of expression of A-type K^+ channels assembled from Kv4.2 and Kv4.3 subunits. Whether these results can be generalized to interneurons in other neuronal circuitries remains to be addressed.

REFERENCES

Baldwin TJ, Tsaur M-L, Lopez GA, Jan YN, Jan LY (1991) Characterization of a mammalian cDNA for an inactivating voltage-sensitive K^+ channel. Neuron 7:471–483.

Chandy KG (1991) Simplified gene nomenclature. Nature 352:26.

Connors BW, Gutnick MJ (1990) Intrinsic firing patterns of diverse neocortical neurons. Trends Neurosci 13:99–104.

Covarrubias M, Wei A, Salkoff L (1991) *Shaker, Shal*, *Shab*, and *Shaw* express independent K^+ current systems. Neuron 7:763–773.

Du J, Zhang L, Weiser M, Rudy B, McBain CJ (1996) Developmental expression and functional characterization of the potassium-channel subunit Kv3.1b in parvalbumin-containing interneurons of the rat hippocampus. J Neurosci 16:506–518.

Ficker E, Heinemann U (1992) Slow and fast transient potassium currents in cultured rat hippocampal cells. J Physiol (Lond) 445:431–455.

Gan L, Perney TM, Kaczmarek LK (1996) Cloning and characterization of the promoter for a potassium channel expressed in high frequency firing neurons. J Biol Chem 271:5859–5865.

Geiger JRP, Melcher T, Koh D-S, Sakmann B, Seeburg PH, Jonas P, Monyer H (1995) Relative abundance of subunit mRNAs determines gating and Ca^{2+} permeability of AMPA receptors in principal neurons and interneurons in rat CNS. Neuron 15:193–204.

Grissmer S, Nguyen AN, Aiyar J, Hanson DC, Mather RJ, Gutman GA, Karmilowicz MJ, Auperin DD, Chandy KG (1994) Pharmacological characterization of five cloned voltage-gated K^+ channels, types Kv1.1, 1.2, 1.3, 1.5, and 3.1, stably expressed in mammalian cell lines. Mol Pharmacol 45:1227–1234.

Han Z-S, Buhl EH, Lörinczi Z, Somogyi P (1993) A high degree of spatial selectivity in the axonal and dendritic domains of physiologically identified local-circuit neurons in the dentate gyrus of the rat hippocampus. Eur J Neurosci 5:395–410.

Hille B (1992) Ionic channels of excitable membranes. Sunderland, MA: Sinauer.

Ho CS, Grange RW, Joho RH (1997) Pleiotropic effects of a disrupted K^+ channel gene: reduced body weight, impaired motor skill and muscle contraction, but no seizures. Proc Natl Acad Sci USA 94:1533–1538.

Jonas P, Bräu ME, Hermsteiner M, Vogel W (1989) Single-channel recording in myelinated nerve fibers reveals one type of Na channel but different K channels. Proc Natl Acad Sci USA 86:7238–7242.

Kanemasa T, Gan L, Perney TM, Wang L-Y, Kaczmarek LK (1995) Electrophysiological and pharmacological characterization of a mammalian *Shaw* channel expressed in NIH 3T3 fibroblasts. J Neurophysiol 74:207–217.

Kirsch GE, Drewe JA (1993) Gating-dependent mechanism of 4-aminopyridine block in two related potassium channels. J Gen Physiol 102:797–816.

Kues WA, Wunder F (1992) Heterogeneous expression patterns of mammalian potassium channel genes in developing and adult rat brain. Eur J Neurosci 4:1296–1308.

Madison DV, Nicoll RA (1984) Control of the repetitive discharge of rat CA1 pyramidal neurones *in vitro*. J Physiol (Lond) 354:319–331.

Maletic-Savatic M, Lenn NJ, Trimmer JS (1995) Differential spatiotemporal expression of K^+ channel polypeptides in rat hippocampal neurons developing *in situ* and *in vitro*. J Neurosci 15:3840–3851.

Martina M, Jonas P (1997) Functional differences in Na^+ channel gating between fast-spiking interneurones and principal neurones of rat hippocampus. J Physiol (Lond) 505:593–603.

Massengill JL, Smith MA, Son DI, O'Dowd DK (1997) Differential expression of $K_{4\text{-}AP}$ currents and Kv3.1 potassium channel transcripts in cortical neurons that develop distinct firing phenotypes. J Neurosci 17:3136–3147.

Monyer H, Jonas P (1995) Polymerase chain reaction analysis of ion channel expression in single neurons of brain slices. In: Single-channel recording (Sakmann B, Neher E, eds), pp 357–373. New York: Plenum.

Moreno H, Kentros C, Bueno E, Weiser M, Hernandez A, Vega-Saenz de Miera E, Ponce A, Thornhill W, Rudy B (1995) Thalamocortical projections have a K^+ channel that is phosphorylated and modulated by cAMP-dependent protein kinase. J Neurosci 15:5486–5501.

Numann RE, Wadman WJ, Wong RKS (1987) Outward currents of single hippocampal cells obtained from the adult guinea-pig. J Physiol (Lond) 393:331–353.

Pak MD, Baker K, Covarrubias M, Butler A, Ratcliffe A, Salkoff L (1991) MShal, a subfamily of A-type K^+ channel cloned from mammalian brain. Proc Natl Acad Sci USA 88:4386–4390.

Pongs O (1992) Molecular biology of voltage-dependent potassium channels. Physiol Rev 72:S69–S88.

Rettig J, Wunder F, Stocker M, Lichtinghagen R, Mastiaux F, Beckh S, Kues W, Pedarzani P, Schröter KH, Ruppersberg JP, Veh R, Pongs O (1992) Characterization of a Shaw-related potassium channel family in rat brain. EMBO J 11:2473–2486.

Ruppersberg JP, Schröter KH, Sakmann B, Stocker M, Sewing S, Pongs O (1990) Heteromultimeric channels formed by rat brain potassium-channel proteins. Nature 345:535–537.

Ruppersberg JP, Stocker M, Pongs O, Heinemann SH, Frank R, Koenen M (1991) Regulation of fast inactivation of cloned mammalian $I_K(A)$ channels by cysteine oxidation. Nature 352:711–714.

Scharfman HE (1995) Electrophysiological diversity of pyramidal-shaped neurons at the granule cell layer/hilus border of the rat dentate gyrus recorded *in vitro*. Hippocampus 5:287–305.

Serôdio P, Rudy B (1998) Differential expression of Kv4 K^+ channel subunits mediating subthreshold transient K^+ (A-type) currents in rat brain. J Neurophysiol 79:1081–1091.

Sewing S, Roeper J, Pongs O (1996) Kvβ1 subunit binding specific for *Shaker*-related potassium channel α subunits. Neuron 16:455–463.

Sheng M, Tsaur M-L, Jan YN, Jan LY (1994) Contrasting subcellular localization of the Kv1.2 K^+ channel subunit in different neurons of rat brain. J Neurosci 14:2408–2417.

Shi G, Kleinklaus AK, Marrion NV, Trimmer JS (1994) Properties of Kv2.1 K^+ channels expressed in transfected mammalian cells. J Biol Chem 269:23204–23211.

Song W-J, Tkatch T, Baranauskas G, Ichinohe N, Kitai ST, Surmeier DJ (1998) Somatodendritic depolarization-activated potassium currents in rat neostriatal cholinergic interneurons are predominantly of the A type and attributable to coexpression of Kv4.2 and Kv4.1 subunits. J Neurosci 18:3124–3137.

Storm JF (1990) Potassium currents in hippocampal pyramidal cells. Prog Brain Res 83:161–187.

Stühmer W, Ruppersberg JP, Schröter KH, Sakmann B, Stocker M, Giese KP, Perschke A, Baumann A, Pongs O (1989) Molecular basis of functional diversity of voltage-gated potassium channels in mammalian brain. EMBO J 8:3235–3244.

Taglialatela M, Vandongen AMJ, Drewe JA, Joho RH, Brown AM, Kirsch GE (1991) Patterns of internal and external tetraethylammonium block in four homologous K^+ channels. Mol Pharmacol 40:299–307.

Talukder G, Harrison NL (1995) On the mechanism of modulation of transient outward current in cultured rat hippocampal neurons by di- and trivalent cations. J Neurophysiol 73:73–79.

Tsaur M-L, Chou C-C, Shih Y-H, Wang H-L (1997) Cloning, expression and CNS distribution of Kv4.3, an A-type K^+ channel α subunit. FEBS Lett 400:215–230.

Weiser M, Vega-Saenz de Miera E, Kentros C, Moreno H, Franzen L, Hillman D, Baker H, Rudy B (1994) Differential expression of *Shaw*-related K^+ channels in the rat central nervous system. J Neurosci 14:949–972.

Weiser M, Bueno E, Sekirnjak C, Martone ME, Baker H, Hillman D, Chen S, Thornhill W, Ellisman M, Rudy B (1995) The potassium channel subunit KV3.1b is localized to somatic and axonal membranes of specific populations of CNS neurons. J Neurosci 15:4298–4314.

Zhang L, McBain CJ (1995a) Voltage-gated potassium currents in stratum oriens-alveus inhibitory neurones of the rat CA1 hippocampus. J Physiol (Lond) 488:647–660.

Zhang L, McBain CJ (1995b) Potassium conductances underlying repolarization and afterhyperpolarization in rat CA1 hippocampal interneurones. J Physiol (Lond) 488:661–672.